Angle dependence of the spontaneous emission from confined optical modes in photonic dots

T. Gutbrod, M. Bayer, and A. Forchel
Technische Physik, Universität Würzburg, Am Hubland, D-97074 Würzburg, Germany

P. A. Knipp
Christopher Newport University, Newport News, Virginia 23606

T. L. Reinecke
Naval Research Laboratory, Washington, D.C. 20375

A. Tartakovskii and V. D. Kulakovskii
Institute of Solid State Physics, Russian Academy of Sciences, 142432 Chernogolovka, Russia

N. A. Gippius and S. G. Tikhodeev
General Physics Institute, Russian Academy of Sciences, 117333 Moscow, Russia
(Received 15 June 1998; revised manuscript received 8 September 1998)

The confined optical modes in photonic dots have been studied by angle-resolved photoluminescence spectroscopy. The photon modes have no dispersion in the cavity plane due to their three-dimensional confinement. The emission intensity from each mode depends strongly on the detection angle. From the angle dependence of the photoluminescence the distribution of the electromagnetic field in the dot plane can be obtained. The experimental findings are in good agreement with theoretical calculations. [S0163-1829(99)08003-0]

I. INTRODUCTION

Semiconductor microcavities have attracted considerable interest in recent years because they permit the control of spontaneous and stimulated emission due to the possibility of tailoring the internal electromagnetic field distribution and of modifying the photon density of states in the cavity.[1–17] For example, in planar two-dimensional microcavities the emission normal to the cavity is strongly suppressed over a broad energy band except for one fundamental resonance around the center of the band. The electromagnetic field is confined along one spatial direction, and the fundamental optical mode is the onset of a continuum of photon modes with free dispersion in the cavity plane.

In order to obtain further control of the emission properties, higher-dimensional photon confinement is useful. Recently, photonic dots have been fabricated in which the photon continuum is split into a set of discrete modes because only modes of certain wave numbers/energies are well confined in the dots.[18,19] The confined modes couple to the continuum of photon modes outside of the dot structures, and they are sharp resonances on the continuum of photon modes in the density of states. In Refs. 18 and 19 the optical modes in photonic dots have been studied by photoluminescence spectroscopy. An increase of the mode energies and of the energy splitting between the modes with decreasing structure size has been found there. These studies, however, give no direct information on the distribution of the electromagnetic fields in the plane of a photonic dot.

Here we have applied angle-resolved photoluminescence spectroscopy to investigate the optical modes in photonic-dot structures. In these experiments the far-field emission of the dots is detected within a small solid angle. The direction of detection is varied relative to the normal of the cavity. Similar angle-resolved spectroscopy recently has been used to study the dispersion relations of the polariton branches in unpatterned microcavities.[6] In such work the energy splitting between the polariton branches, the so-called Rabi-splitting, can be determined from the experiments.

In photonic dots the electromagnetic-field pattern of each optical mode causes a characteristic emission-intensity profile for varying directions of detection. Thus, angle-resolved studies allow us to determine the field distributions in the dots. Further, we have calculated the far-field emission intensities from each photonic-dot mode and compared these results with the experimental data. The paper is organized as follows: In the next section we present the photonic-dot structures studied in the present experiments. The experimental results are shown in Sec. III and compared to the model calculations in Sec. IV.

II. PHOTONIC DOTS

A conventional λ-cavity consisting of a GaAs layer with a height of 251 nm sandwiched between two high-reflectance GaAs/AlAs mirrors was used for the fabrication of photonic dots. In the center of the GaAs layer a 7-nm-wide $In_{0.14}Ga_{0.86}As$ quantum well was placed as an optically active medium. In order to obtain three-dimensional photon confinement, square-shaped columns were fabricated from the two-dimensional cavity by lithography and etching. Details of the fabrication process have been given elsewhere.[20] The cavity was etched through the top reflector and the GaAs layer down to the top of the bottom reflector. The lateral sizes of the dots were determined from scanning electron microscopy and ranged from 6 μm down to 2.7 μm.

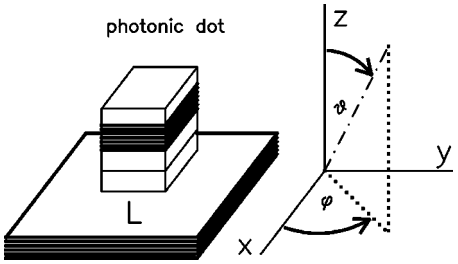

FIG. 1. Definition of the polar angle ϑ and the azimuthal angle φ characterizing the spatial direction along which the emission of the photonic dots is detected.

The samples were mounted into the Helium insert of an optical cryostat at $T=5$ K. An Ar^+ laser was used for optical excitation of the cavities. In the angle-resolved experiments only the emission within a narrow solid angle is detected by using an aperture, which could be moved parallel to the cavity plane. The aperture is located far from the photonic-dot structures. With a sample-aperture distance of 20 cm and an aperture diameter of 4 mm an angle resolution of about 1° is obtained. Each direction of detection is uniquely defined by a set of two angles, the polar angle ϑ (angle to the cavity normal) and the azimuthal angle φ (angle in the cavity plane) as shown schematically in Fig. 1. Each set of angles corresponds to in-plane photon wave vectors $k_x=k\sin\vartheta\cos\varphi$ and $k_y=k\sin\vartheta\sin\varphi$, where k is the photon wave number. The detection angle inside and outside the cavity, ϑ_{in} and ϑ are connected to each other by the law of diffraction, $\sqrt{\varepsilon}\sin(\vartheta_{in})=\sin(\vartheta)$ with the dielectric constant ε. The emission was dispersed by a double monochromator with a focal length of 1 m and detected by a Peltier-cooled GaAs photomultiplier interfaced with a photon counting system.

III. EXPERIMENTAL RESULTS

In an unpatterned cavity the photon modes have free dispersion in the cavity plane with their energies given by

$$E(k_\parallel)=\sqrt{E_0^2+\frac{\hbar^2c_0^2}{\varepsilon}k_\parallel^2}, \tag{1}$$

where $E_0=\hbar ck_0/\sqrt{\varepsilon}$ is the energy of the fundamental cavity mode determined by the height of the GaAs λ cavity and $k_\parallel=\sqrt{k_x^2+k_y^2}$ is the photon wave number in the cavity plane.

In photonic dots three-dimensional photon confinement is obtained, and the dispersion of the photon modes in the cavity plane is suppressed due to the discontinuity of the refractive index at the lateral sidewalls. Detailed calculations of the energies of the modes in these structures have been made and shown to be in good agreement with the experiment.[19] They show that the energies of the photon modes (n_x,n_y) are given to a good approximation by the formula

$$E_{n_x,n_y}=\sqrt{E_0^2+\frac{\hbar^2c_0^2}{\varepsilon}(q_{n_x}^2+q_{n_y}^2)}, \tag{2}$$

with the confined photon wave numbers $q_{n_i}=(\pi/L)(n_i+1)$, $i=x,y$ and $n_i=0,1,\ldots$. Here the modes are standing waves in square microcavities of size L. To describe the experimental energies with Eq. (1), the size L has to be somewhat larger than the physical size due to the penetration of the fields into the vacuum and into the lower mirror.

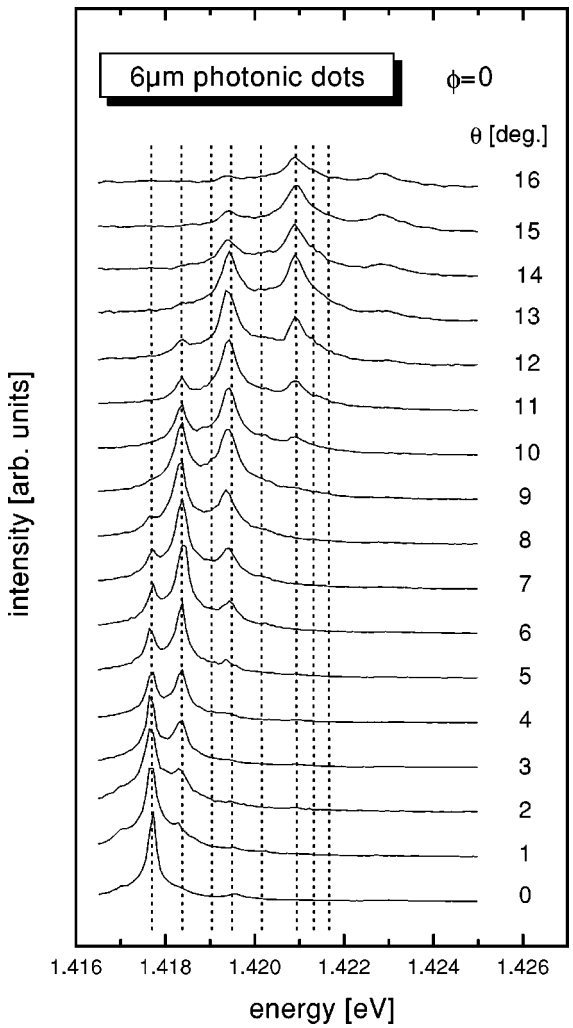

FIG. 2. Angle-resolved spectra of a photonic dot with a size 6 μm. The polar angle ϑ was varied for a fixed azimuthal angle $\varphi=0$.

The eigenvalues n_x and n_y give the number of nodes in the electromagnetic-field distributions along the x and y direction, respectively. Each mode can be characterized by its parities, either even or odd, $P_x=(-1)^{n_x}$ and $P_y=(-1)^{n_y}$. Modes with $n_x\neq n_y$ are twofold degenerate[21] due to the square symmetry of the dot structures, while modes with $n_x=n_y$ are nondegenerate. The degenerate modes can be transformed into each other by rotations of 90°. The order in energy of the eight lowest modes is (0,0), (1,0), (1,1), (2,0), (2,1), (3,0), (2,2), and (3,1).

In Fig. 2 angle-resolved photoluminescence spectra of photonic dots with a lateral size of 6 μm are shown. For these spectra the azimuthal angle was fixed at $\varphi=0$ and the polar angle ϑ was varied from 0 to 16°. The exciton mode is not shown because its energy is more than 15 meV smaller than the energy of the cavity modes.[22,23] This energy separation is so large that the optical modes are only weakly coupled to the electron-hole continuum of states. Several laterally confined photon modes are observed when varying ϑ. The energies of the photon modes do not vary with ϑ, giving

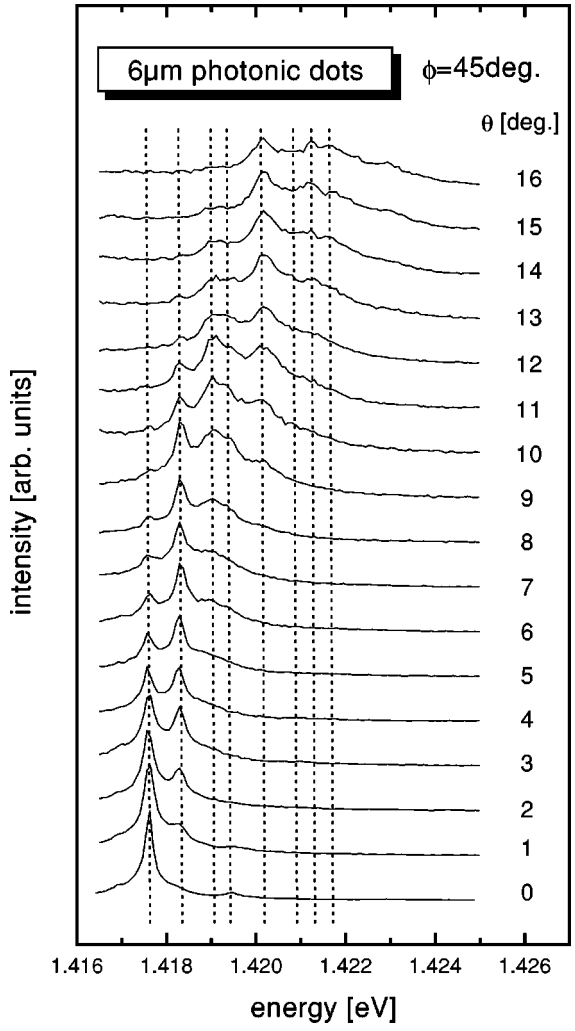

FIG. 3. Angle-resolved spectra of a photonic dot with a size 6 μm. The polar angle ϑ was varied as in Fig. 2 for a fixed azimuthal angle $\varphi=45°$.

clear evidence for their confinement in the cavity plane. However, the emission intensity from each mode depends strongly on the detection angle. For example, the emission of the ground photon mode (0,0) is maximum for $\vartheta=0$ and drops to zero with increasing ϑ. For angles $\vartheta>8°$ ground-mode emission is no longer detected. The first excited mode (1,0) which is degenerate with (0,1) (Ref. 21) cannot be observed at $\vartheta=0$. With the increasing detection angle its intensity rises from zero, has a maximum at about $\vartheta=6°$, and then drops again to zero.

The dotted lines in Fig. 2 indicate the calculated energies of the photon modes in 6-μm-wide dots. For the two lowest photon modes good agreement with the experiment is observed. However, at the energy at which emission from the second excited mode (1,1) is expected, no emission is observed in the spectra for a dot orientation $\varphi=0$. In contrast, luminescence is observed at the energy where the next higher- lying mode (2,0) is located. This mode has a small emission intensity for $\vartheta=0$, which decreases with increasing ϑ, is zero at about $\vartheta=3°$, then increases again and has a maximum for $\vartheta=11°$. Out of the next four higher-lying modes only one [(3,0)] has a large emission intensity for $\varphi=0$, while from the other modes only weak emission is detected.

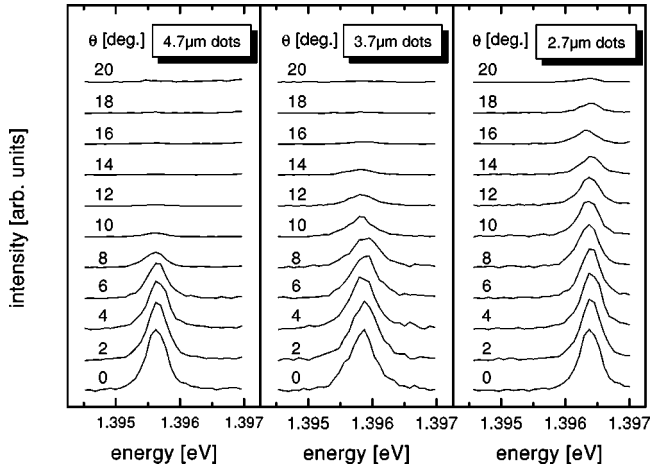

FIG. 4. Angle resolved spectra of the ground photon-mode emission in photonic dots with varying lateral sizes, 4.7 μm, 3.7 μm, and 2.7 μm. The orientation of the dot was $\varphi=0$.

For comparison, also angle-resolved spectra of a 6-μm-wide photonic dot have been recorded with the azimuthal angle fixed at $\varphi=45°$. These spectra are shown in Fig. 3. The behavior of the modes (0,0), (1,0), and (2,0) is similar to the behavior at $\varphi=0$. But for this dot orientation emission is observed also at energies at which the mode (1,1) is expected from the calculations. Its intensity is zero at $\vartheta=0$, then it increases, has a maximum at about $\vartheta=9°$, and for larger angles it drops to zero. For this orientation of the photonic dot significant emission from the three higher-lying modes (2,1), (2,2), and (3,1) also is detected, which were hardly observable at $\varphi=0$. In contrast, the emission from the mode (3,0) is strongly reduced.

The solid angle into which the several photon modes emit with appreciable intensity depends on the size of the dot. Figure 4 shows angle-resolved luminescence spectra of the ground-photon mode (0,0) for cavity sizes of 4.7, 3.7, and 2.7 μm. The detection angle is varied up to 20° in steps of 2°. Qualitatively, the angle dependence is similar in all three cases. Quantitatively, however, the emission is distributed over a larger range of angles ϑ, the smaller the cavity size. For the 4.7-μm-wide cavities the emission has dropped to zero already for $\vartheta>10°$, for the 3.7-μm-wide dots it becomes zero at $\vartheta>14°$, and for the 2.7-μm-wide ones it is zero for angles larger than 20°. As discussed above, in a 6-μm-wide dot (0,0) emission was no longer observable already at $\vartheta>8°$.

IV. DISCUSSION

The calculation of the far-field emission of a photonic dot is similar to that of diffraction of an electromagnetic wave at a square aperture of size L. In the case of the Fraunhofer diffraction, where the signal is detected far from the aperture, the interference pattern is given by the Fourier-transform of the aperture function. Therefore, the electromagnetic field far from the photonic dot is given by the Fourier transform of the field in the cavity plane. For the field distribution $\mathcal{E}_{n_x,n_y}(x,y)$ in the photonic dot the intensity distribution at the detector is given by[24]

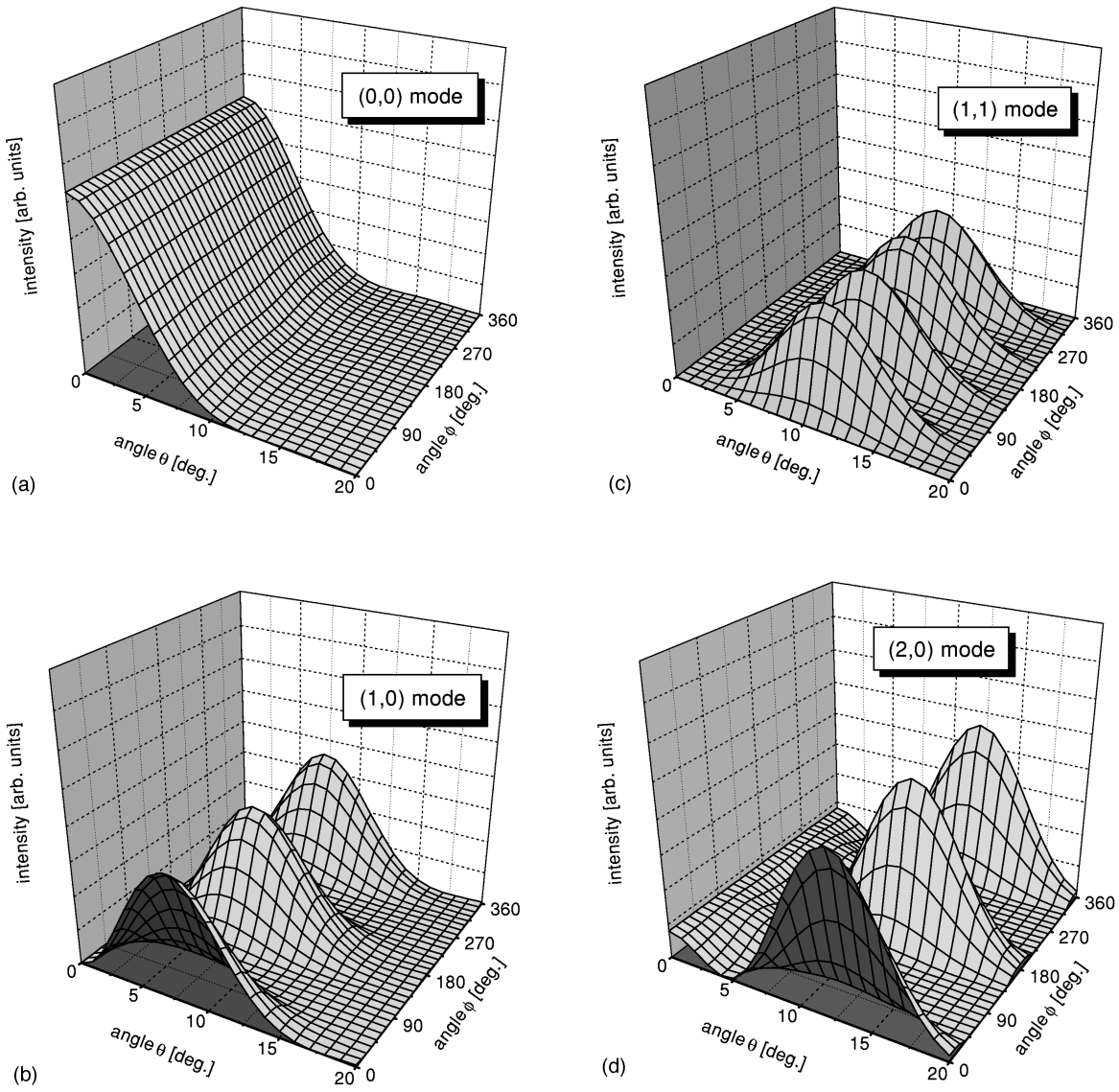

FIG. 5. Far-field emission intensity of the four lowest modes in 6-μm-wide photonic dots plotted vs the polar angle ϑ and the azimuthal angle φ. Intensity for the (0,0) mode (a), for the (1,0) (b), the (1,1) mode (c), and for the (2,0) mode (d).

$$I_{n_x,n_y}(\vartheta,\varphi)=\left|\int \mathcal{E}_{n_x,n_y}(x,y)\exp[i(k_x x+k_y y)]dxdy\right|^2, \tag{3}$$

with $k_x=k\sin\vartheta\cos\varphi$ and $k_y=k\sin\vartheta\sin\varphi$.[25]

The electromagnetic fields are well confined inside of the photonic dots with a dot size of 6 μm, because the field amplitudes are about zero at the boundaries of the dots. Therefore, to a good approximation Maxwell's equations can be separated in the x and y coordinates and the fields can be approximated by those in a cavity with perfectly reflecting sidewalls, $\mathcal{E}_{n_x,n_y}(x,y)=\mathcal{E}_{n_x}(x)\mathcal{E}_{n_y}(y)$ with

$$\mathcal{E}_{n_i}(i)\sim\cos(q_{n_i}i) \tag{4}$$

for modes of even parity along the direction $i, i=x,y$ and

$$\mathcal{E}_{n_i}(i)\sim\sin(q_{n_i}i) \tag{5}$$

for modes of odd parity. The q_{n_i} are the confined-photon wave numbers in Eq. (2). From these field distributions the far-field emission intensities can be calculated analytically. The emission intensities are given by $I_{n_x,n_y}(\vartheta,\varphi)=I_{n_x}(k_x)I_{n_y}(k_y)$, where the $I_{n_i}(k_i)$ for modes of even parity are given by

$$I_{n_i}(k_i)\sim\frac{q_{n_i}^2}{(q_{n_i}^2-k_i^2)^2}\left[\cos\left(\frac{L}{2}k_i\right)\right]^2, \tag{6}$$

and for modes of odd parities by

$$I_{n_i}(k_i)\sim\frac{q_{n_i}^2}{(q_{n_i}^2-k_i^2)^2}\left[\sin\left(\frac{L}{2}k_i\right)\right]^2. \tag{7}$$

Thus, each intensity distribution $I_{n_i}(k_i)$ is a product of two factors.

(i) The first factor is a form factor and gives the amplitude of the intensity with observation direction. Maximum intensity occurs when the direction of detection coincides with the photon wave vector. These directions are given by

$k \sin\vartheta \cos\varphi = (\pi/L)(n_x+1)$ and $k \sin\vartheta \sin\varphi = (\pi/L)(n_y+1)$. Therefore, for a fixed-dot orientation φ the maximum of the emission is shifted to larger angles ϑ, the larger the lateral wave number $k_\parallel = \sqrt{k_x^2 + k_y^2}$ of the involved dot mode is. This maximum clearly dominates the emission from each mode.

(ii) The second factor gives the modulation of the emission intensity with the direction of detection (ϑ, φ) and is periodic in φ and ϑ. This factor also determines the shape of the far-field emission pattern through the parities of the modes. Only for modes with even symmetry along the x and y directions, emission can be observed at $\vartheta = 0$, normal to the dot. For modes with odd symmetry along one direction, the field contributions to the far-field emission interfere destructively.

Figure 5 shows three-dimensional plots of the intensities of the four lowest photon modes as functions of the polar angle ϑ and the azimuthal angle φ. The dot size is 6 μm. In addition, these intensities for fixed-dot orientations of $\varphi = 0$ and $\varphi = 45°$ are compared to the experimental data in Figs. 6 and 7 for the eight lowest-confined modes.[26,27] There, symbols give the experimental data (squares for $\varphi = 0$ and circles for $\varphi = 45°$) and lines show the results of the calculations (solid lines for $\varphi = 0$ and dotted ones for $\varphi = 45°$). The absolute-emission intensity from each mode depends strongly on the coupling of each optical mode to the electronic states in the quantum well and cannot be easily compared with each other. Therefore, the maximum intensity of each mode has been normalized to unity.

The emission of the ground-photon mode has almost no dependence on the orientation φ of the photonic dot. It is maximum for $\vartheta = 0$ and then decreases. The intensities of the side maxima are so small that they cannot be resolved experimentally. From the calculations we find that, e.g., the first side maximum of the (0,0) mode is located at about 20°. Its intensity is, however, only 2% of that of the main maximum. The intensities of higher-order maxima are even smaller. Therefore, the ground-photon mode mainly consists of Fourier components with wave numbers around zero.

The electric-field distributions of the higher-confined optical modes are increasingly modulated in the plane of the photonic dot. Therefore, higher Fourier components become important for these photon modes resulting in the shift of the main-emission maximum to larger angles, i.e., larger in-plane wave numbers. Further, for these modes the relative intensities of the side maxima increase.

For the first excited mode (1,0) the emission depends on the orientation of the dot. When measuring along the y direction ($\varphi = 90°$, parallel to the node plane of the mode) the electric-field contributions to the far-field emission interfere destructively for all angles ϑ [Fig. 5(b)]. In contrast, when measuring along the x direction ($\varphi = 0$, normal to the node plane) emission is observed. However, the mode (1,0) is degenerate with the mode (0,1),[21] and the far-field distribution of the latter mode is obtained from that of (1,0) by a rotation of 90° around the z axis. When adding the two distributions, the emission intensity depends only weakly on φ. For example, it is maximum for $\varphi = 0$, drops by about 20% up to $\varphi = 45°$ [shown in Fig. 6(b)] and then increases to reach again maximum intensity for $\varphi = 90°$.

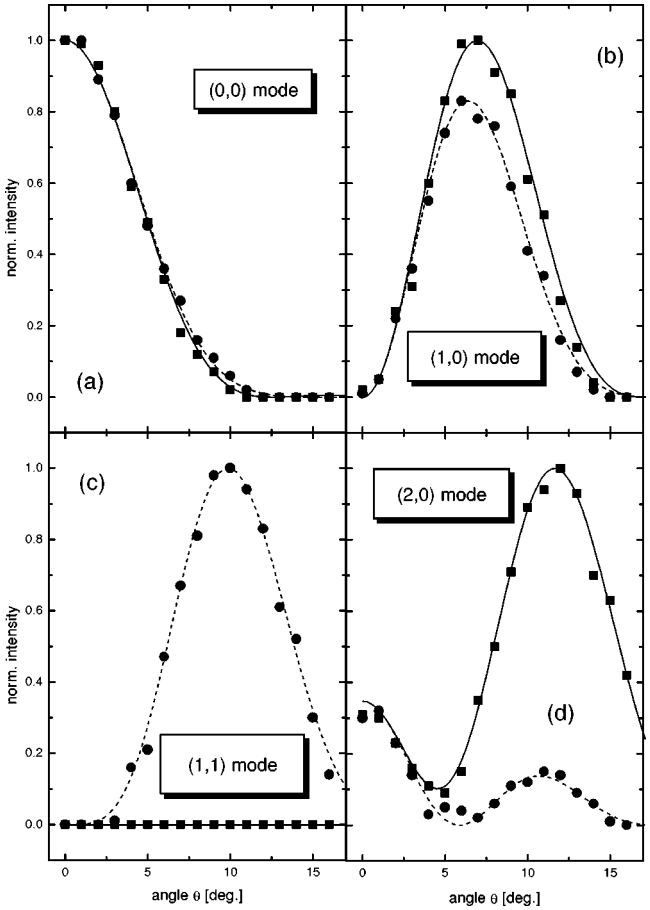

FIG. 6. Emission intenities of the optical modes in a 6-μm-wide photonic dot as functions of ϑ. The dot orientation was $\varphi = 0$ and $\varphi = 45°$. Data for the (0,0) mode (a), for the (1,0) (b), the (1,1) mode (c), and for the (2,0) mode (d). Lines give the results of calculations (solid lines for $\varphi = 0$, dotted ones for $\varphi = 45°$), symbols the experimental data (squares for $\varphi = 0$, circles for $\varphi = 45°$).

The next higher-lying mode (1,1) is nondegenerate. Because of its modulation along both spatial directions in the cavity plane the emission varies more strongly with φ as compared to the (1,0) mode. For the orientation $\varphi = 0$ no emission is observed because the fields cancel each other at the detector for all ϑ. When the orientation of the dot is changed by 45°, emission from this mode becomes observable.

The intensity of the (2,0) mode is nonzero at $\vartheta = 0$ because of even parities along the x and y directions leading to constructive interference of the fields. For larger angles the behavior is similar to that observed for the (1,0) mode. However, when adding the intensity distribution of the degenerate (0,2) mode, the modulation with φ is significantly stronger than in the case of the total intensity of the (1,0) and (0,1) modes.

The width of the main maximum in the Fourier transform of the field distribution increases with decreasing structure size. E.g., in the case of (0,0) Fourier components with larger wave numbers are mixed into the mode when its spatial confinement becomes stronger. This can be seen from Fig. 8, where the (0,0) emission intensity is plotted against ϑ for various dot sizes, 6 μm, 4.7 μm, 3.7 μm, and 2.7 μm. Qualitatively, the behavior of the emission is the same for all

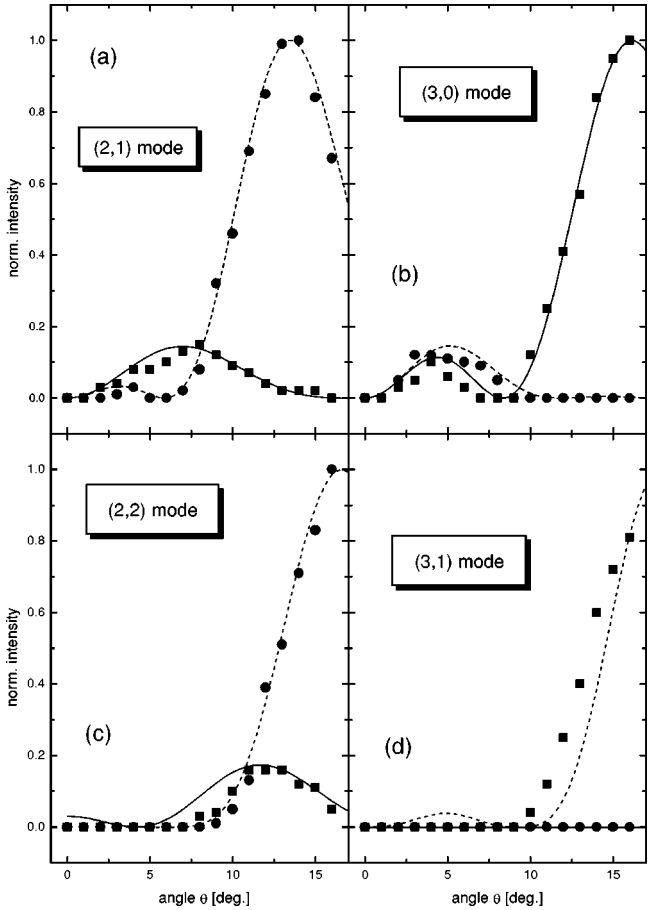

FIG. 7. Same as Fig. 8, but data for the (2,1) mode (a), for the (3,0) mode (b), for the (2,2) mode (c), and for the (3,1) mode (d).

dot sizes. Quantitatively, the solid angle of the emission increases with decreasing structure size. From our calculations we find that this solid angle increases with $1/L$ with decreasing structure size. This behavior is well reproduced by the experimental data.

V. SUMMARY

In summary, we have studied the electromagnetic-field distributions of the optical modes in photonic dots using angle-resolved photoluminescence spectroscopy. We have shown that these studies give directly the spatial Fourier transforms of the electric-field distributions in the cavities. The experimental results for the angular dependences are in good agreement with calculations of the electric-field distributions. Therefore, we have obtained a quantitative picture of these electric-field distributions of the modes themselves.

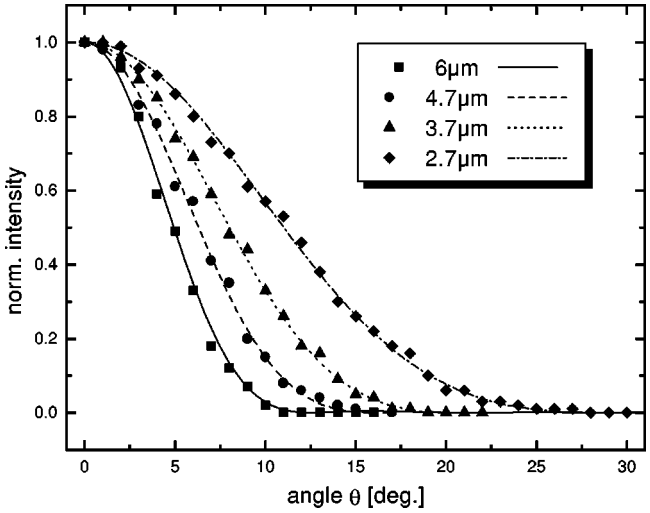

FIG. 8. Emission intenities of the ground-optical mode (0,0) in photonic dots of varying sizes as functions of ϑ. The dot orientation was $\varphi = 0°$. Symbols give the experimental data, lines the calculated results.

This situation might be contrasted with that of the wave functions of electronic states in nanometer-sized quantum dots, which have attracted much attention in recent years. In that case there are no measurements of the states that give direct insight about the wave functions on a scale similar to that presented here for the modes of photonic dots. In addition, in the case of electronic quantum dots there often are uncertainties in the models used, such as electron-electron many-body effects, damages at interfaces or uncertainties in the potentials, which limit the reliability of the understanding of their states based on comparison of calculated energies with experimental results. The detailed results for the present photonic dots may make them attractive both for further fundamental studies in, e.g., optical couplings to electronic excitations or more complex structures made from them, or for potential applications such as in lasers with reduced-spontaneous emission.

ACKNOWLEDGMENTS

This work was supported by the State of Bavaria, the Deutsche Forschungsgemeinschaft, the Volkswagen-Stiftung, INTAS, and the U.S. Office of Naval Research.

[1] H. Yokoyama, K. Nishi, T. Anan, H. Yamada, S. D. Brorson, and E. P. Ippen, Appl. Phys. Lett. **57**, 2814 (1990).
[2] G. Björk, S. Machida, Y. Yamamoto, and K. Igeta, Phys. Rev. A **44**, 669 (1991).
[3] C. Weisbuch, M. Nishioka, A. Ishikawa, and Y. Arakawa, Phys. Rev. Lett. **69**, 3314 (1992).
[4] R. P. Stanley, R. Houdré, U. Oesterle, M. Ilegems, and C. Weisbuch, Phys. Rev. A **48**, 2246 (1993).
[5] V. Savona, Z. Hradil, A. Quattropani, and P. Schwendimann, Phys. Rev. B **49**, 8774 (1994).
[6] R. Houdré, C. Weisbuch, R. P. Stanley, U. Oesterle, P. Pellandini, and M. Ilegems, Phys. Rev. Lett. **73**, 2043 (1994).
[7] I. Abram and J. L. Oudar, Phys. Rev. A **51**, 4116 (1995).
[8] H. Wang, J. Shah, T. C. Damen, W. Y. Jan, J. E. Cunningham, M. Hong, and J. P. Mannaerts, Phys. Rev. B **51**, 14 713 (1995).
[9] R. Houdré, J. L. Gibernon, P. Pellandini, R. P. Stanley, U. Oesterle, C. Weisbuch, J. O'Gorman, B. Roycroft, and M. Ilegems, Phys. Rev. B **52**, 7810 (1995).
[10] F. Tassone, C. Piermarocchi, V. Savona, A. Quattropani, and P. Schwendimann, Phys. Rev. B **53**, 7642 (1996).

[11] R. P. Stanley, R. Houdré, C. Weisbuch, U. Oesterle, and M. Ilegems, Phys. Rev. B **53**, 10 995 (1996).
[12] V. Savona, F. Tassone, C. Piermarocchi, A. Quattropani, and P. Schwerdimann, Phys. Rev. B **53**, 13 051 (1996).
[13] P. Kinsler and D. M. Whittaker, Phys. Rev. B **54**, 4988 (1996).
[14] D. M. Whittaker, P. Kinsler, T. A. Fisher, M. S. Skolnick, A. Armitage, A. M. Afshar, M. D. Sturge, J. S. Roberts, G. Hill, and M. A. Pate, Phys. Rev. Lett. **77**, 4792 (1996).
[15] F. Jahnke, M. Kira, S. W. Koch, G. Khitrova, E. K. Lindmark, T. R. Nelson Jr., D. V. Wick, J. D. Berger, O. Lyngnes, H. M. Gibbs, and K. Tai, Phys. Rev. Lett. **77**, 5257 (1996).
[16] A. Armitage, T. A. Fisher, M. S. Skolnick, D. M. Whittaker, P. Kinsler, and J. S. Roberts, Phys. Rev. B **55**, 16 395 (1997).
[17] D. Baxter, M. S. Skolnick, A. Armitage, V. N. Astratov, D. M. Whittaker, T. A. Fisher, J. S. Roberts, D. J. Mowbray, and M. A. Kaliteevski, Phys. Rev. B **56**, 10 032 (1997).
[18] J. M. Gérard, D. Barrier, J. Y. Marzin, R. Kuszelewicz, L. Manin, E. Costard, V. Thierry-Mieg, and T. Rivera, Appl. Phys. Lett. **69**, 449 (1996).
[19] J. P. Reithmaier, M. Röhner, H. Zull, F. Schäfer, A. Forchel, P. A. Knipp, and T. L. Reinecke, Phys. Rev. Lett. **78**, 378 (1997).
[20] M. Röhner, J. P. Reithmaier, A. Forchel, F. Schäfer, and H. Zull, Appl. Phys. Lett. **71**, 488 (1997).
[21] The polarizations of the electromagnetic modes will not be considered in detail here. In case of the ground mode the two independent polarizations are degenerate with each other. Each of the two first-excited modes (1,0) and (0,1) is split into a doublet because of the different boundary conditions at the semiconductor-vacuum interface for the two polarizations. However, from the full calculations we find that this polarization splitting is rather small in the case of the present structures. For example, for a 4.7-μm-wide dot the splitting is 0.06 meV, for a 2.3-μm-wide dot it is 0.5 meV.
[22] The in-plane dispersion of the exciton is given by the center-of-mass motion of the exciton, whose energy depends only weakly on the observation direction in comparison to the photon mode.
[23] The halfwidth of the photon-mode emission increases continuously with increasing polar angle. This increase can be attibuted to the decrease of reflectivity of the two Bragg reflectors with increasing ϑ.
[24] See, for example, E. Hecht and A. Zajac, *Optics* (Addison-Wesley, Reading, MA, 1974).
[25] For diffraction of a plane wave at a square aperture, each point of the aperture is the origin of a spherical wave. The amplitude of each of these elementary waves is equal. In case of the photonic dots the amplitude of each of these elementary waves is given by the local electromagnetic field in the photonic dot.
[26] For the higher-lying, closely spaced modes, in particular (2,2) and (3,1), the intensities have been determined from a lineshape analysis, for which the calculated mode energies have been used. For the spectral linewidth we have taken the values from other modes, which are located closely in energy.
[27] For different dot orientations the exciton luminescence is normalized to the same value first and then the emission intensities of the optical modes are compared with each other.